

Phase Harmonics and Correlation Invariants in Convolutional Neural Networks

Stéphane Mallat^{1,2}, Sixin Zhang^{2,3} and Gaspar Rochette^{2*}

¹ *Collège de France, 75005 Paris, France*

² *École Normale Supérieure, PSL, Paris*

³ *Center for Data Science, Peking University, Beijing, China*

July 16, 2022

Abstract

We prove that linear rectifiers act as phase transformations on complex analytic extensions of convolutional network coefficients. These phase transformations are linearized over a set of phase harmonics, computed with a Fourier transform. The correlation matrix of one-layer convolutional network coefficients is a translation invariant representation, which is used to build statistical models of stationary processes. We prove that it is Lipschitz continuous and that it has a sparse representation over phase harmonics. When network filters are wavelets, phase harmonic correlations provide important information about phase alignments across scales. We demonstrate numerically that large classes of one-dimensional signals and images are precisely reconstructed with a small fraction of phase harmonic correlations.

1 Introduction

The responses of convolutional neural networks are difficult to analyze because of their non-linearities. We concentrate on linear rectifiers which are most often used [7]. Eventhough linear rectifiers are applied to real coefficients, we show that these non-linear operators act as a transformation of a

*This work is supported by the ERC InvariantClass 320959

complex phase, defined by an analytic extension of network filters. We prove that phase transformations are linearized over phase harmonics computed with a Fourier transform. Phase harmonics provide a new approach to correlate phase information, and we shall see that they play an important role in multiscale representations, to relate structures across scales.

Gatys et. al. [4] have shown that correlations of deep convolutional network layers, trained on a supervised learning task, can provide rich descriptors to generate stationary image textures. The correlation descriptors are invariant to translations of the input signal. They have also been applied to audio signal generations by Chorowski et. al. [3]. However, Ustyuzhaninov et. al. [15] showed that filters do not need to be learned and that depth is not crucial. They generate image textures of similar quality by correlating the coefficients of a shallow one-layer convolutional network, calculated with multiscale random filters or multiscale windowed cosine filters. We show that phase harmonics correlations provide a sparse representation of these shallow network correlations, and we prove that these correlation matrices satisfy Lipschitz continuity bounds.

Rather than using multiscale random or cosine filters, we shall use wavelet filters, whose properties are well understood. The phase of wavelet coefficients is known to carry important information on singularities of one-dimensional signals [1] and on the geometry of edges in images [9]. The modulus and the phase of wavelet coefficients have been used by Portilla and Simoncelli [12] to synthesis complex image textures. We show that wavelet phase harmonic correlations capture phase alignments across scales. Rather than reconstructing “similar” textures as in [15, 12], we study the exact reconstruction of signals from multiscale wavelet phase harmonic correlations, up to a global translation. We demonstrate numerically that large classes of one-dimensional signals and images are precisely recovered from a relatively small fraction of these phase harmonic correlations.

Section 2 begins by defining the complex phase of analytic filter extensions, and explains why linear rectifiers act as a phase transformation. We introduce phase harmonics computed with a Fourier transform and prove that these phase harmonics linearize all homogeneous pointwise operators, including linear rectifiers. Section 3 introduces integral and correlation invariants computed over a one-layer convolutional network. It proves that phase harmonics integrals and correlations are Lipschitz continuous to additive perturbations. Section 4 considers one-layer convolutional networks computed with wavelet filters, for one and two-dimensional signals. We in-

introduce a new complex bump wavelet which is a C^∞ function, with a fast decay and which has an infinite number of vanishing moments. Section 5 demonstrates numerically that large classes of one and two dimensional signals can be reconstructed up to a global translation, from a limited number of wavelet phase harmonic correlations.

Notations: We write $\varphi(z)$ the complex phase of $z \in \mathbb{C}$. For any $x \in \mathbf{L}^2(\mathbb{R}^d)$, we write $\|x\|^2 = \int_{\mathbb{R}^d} |x(u)|^2 du$. The Fourier transform of $x(u)$ is written $\widehat{x}(\omega) = \int_{\mathbb{R}^d} x(u) e^{-i\omega \cdot u} du$.

2 Phases in Convolutional Networks

2.1 Linear Rectifiers as Phase Transformations

A one-layer convolutional network computes convolutions of the input signal x with a family of real valued filters ψ_k^r and applies a pointwise transformation $\rho(x \star \psi_k^r)$, which most often is a linear rectifier $\rho(a) = \max(a, 0)$. We show that these linear rectifiers act as transformations of a complex analytical phase.

We associate a complex analytic filter with a phase to each real filter ψ_k^r . In one dimension $u \in \mathbb{R}$, a real filter $\psi_k^r(u)$ can be written

$$\psi_k^r = \text{Real}(e^{i\alpha} \psi_\lambda) \quad (1)$$

where the complex analytic filter ψ_λ has a Fourier transform which is zero at negative frequencies

$$\widehat{\psi}_\lambda(\omega) = 2 e^{-i\alpha} \widehat{\psi}_k^r(\omega) 1_{[0, \infty)}(\omega) . \quad (2)$$

We define the index λ to be the positive center frequency of $\widehat{\psi}_k^r$ given by

$$\lambda = \frac{\int_{\mathbb{R}^+} \omega |\widehat{\psi}_k^r(\omega)|^2 d\omega}{\int_{\mathbb{R}^+} |\widehat{\psi}_k^r(\omega)|^2 d\omega}, \quad (3)$$

and we impose that $\widehat{\psi}_\lambda(\lambda)$ is real and positive. The phase α is thus the complex phase of $\widehat{\psi}_k^r(\lambda)$. We verify (1) by observing that $\widehat{\psi}_k^r(-\omega) = \widehat{\psi}_k^r(\omega)^*$ because ψ_k^r is real.

In multiple dimensions $u \in \mathbb{R}^d$, the analytic extension of ψ_k^r is a complex filter ψ_λ which is not uniquely defined, but can be written

$$\widehat{\psi}_\lambda(\omega) = 2 e^{-i\alpha} \widehat{\psi}_k^r(\omega) 1_{H_k}(\omega)$$

where H_k is a half space of \mathbb{R}^d whose boundary is a hyperplane including the frequency 0. If possible, the half space H_k is chosen so that $\widehat{\psi}_k^r(\omega) = 0$ for all ω in the boundary of H_k , so that $\widehat{\psi}_\lambda(\omega)$ is not discontinuous at these boundary points. The center frequency λ is defined by replacing the integrals over \mathbb{R}^+ by integrals over H_k in (3) and α is the complex phase of $\widehat{\psi}_k^r(\lambda)$.

Since $\psi_k^r = \text{Real}(e^{i\alpha} \psi_\lambda)$, with no loss of generality we can replace the index k by the phase α and center frequency λ . It provides a more natural topology over the network coefficients $\rho(x \star \psi_k^r(u))$, which are rewritten

$$Ux(u, \alpha, \lambda) = \rho(x \star \text{Real}(e^{i\alpha} \psi_\lambda(u))) = \rho(\text{Real}(x \star e^{i\alpha} \psi_\lambda(u))). \quad (4)$$

Observe that a linear rectifier $\rho(a) = \max(a, 0)$ is a homogeneous operator, which means that

$$\forall(\beta, a) \in \mathbb{R}^+ \times \mathbb{R} \quad , \quad \rho(\beta a) = \beta \rho(a).$$

An absolute value $\rho(a) = |a|$ and the identity $\rho(a) = a$ are also homogeneous. A homogeneous operator ρ acts as a phase transformation. Indeed, for any $z = |z| e^{i\varphi(z)} \in \mathbb{C}$

$$\rho(\text{Real}(z)) = |z| \rho(\cos(\varphi(z))).$$

Applied to $z = e^{i\alpha} x \star \psi_\lambda(u)$ in (4), it proves that

$$Ux(u, \alpha, \lambda) = |x \star \psi_\lambda(u)| \gamma(\varphi(x \star \psi_\lambda(u)) + \alpha) , \quad (5)$$

where

$$\gamma(\alpha) = \rho(\cos(\alpha)) . \quad (6)$$

The function γ is a phase transformation, which is 2π periodic and even. It depends upon ρ . For a linear rectifier, $\gamma(\alpha) = \max(\cos \alpha, 0)$, for an absolute value $\gamma(\alpha) = |\cos \alpha|$ and for the identity $\gamma(\alpha) = \cos \alpha$.

2.2 Linearized Transformation over Phase Harmonics

We prove that the phase transformation induced by a homogeneous non-linearity becomes a linear multiplicative operator over phase harmonics. These harmonics are calculated with a Fourier transform along phases.

We saw in (5) that convolutional network coefficients can be written:

$$Ux(u, \alpha, \lambda) = |x \star \psi_\lambda(u)| \gamma(\varphi(x \star \psi_\lambda(u)) + \alpha) , \quad (7)$$

so one can factorize

$$U = \Gamma W \quad (8)$$

where W computes linear convolutions

$$Wx(u, \lambda) = x \star \psi_\lambda(u) \quad \text{for } \lambda \in \Lambda ,$$

and Γ is the phase transformation

$$\forall z \in \mathbb{C} , \quad \Gamma z(\alpha) = |z| \gamma(\varphi(z) + \alpha) . \quad (9)$$

The following definition introduces the notion of phase harmonics. As opposed to usual complex analysis, the exponent is not applied to the modulus but to the phase only

Definition 2.1 *The phase harmonics of a complex number $z \in \mathbb{C}$ is a sequence defined for all $k \in \mathbb{Z}$ by*

$$[z]^k = |z| e^{ik\varphi(z)} .$$

The Fourier coefficients of a 2π periodic function $\gamma(\alpha)$ are written

$$\widehat{\gamma}(k) = \frac{1}{2\pi} \int_0^{2\pi} \gamma(\alpha) e^{-ik\alpha} d\alpha .$$

The following proposition proves that the Fourier transform $\Gamma z(\alpha)$ is proportional to the phase harmonic sequence of z

Proposition 2.1 *For all $z \in \mathbb{C}$, the Fourier coefficients of $\Gamma z(\alpha)$ is*

$$\widehat{\Gamma} z(k) = \widehat{\gamma}(k) [z]^k . \quad (10)$$

The Fourier transform of $Ux(u, \alpha, \lambda)$ along α is

$$\widehat{U} x(u, k, \lambda) = \widehat{\gamma}(k) [x \star \psi_\lambda(u)]^k . \quad (11)$$

Equation (10) and (11) are directly obtained by computing the Fourier transform of (9) and (7) along α . Equation (11) proves that the phase transformation of a homogeneous non-linearity is a linear multiplicative operator over phase harmonics.

The choice of ρ modifies γ and hence the multipliers $\widehat{\gamma}(k)$. If $\rho(a) = a$ then $\gamma = \cos \alpha$ so $\widehat{\gamma}(k) = 1/2$ if $k = \pm 1$ and $\widehat{\gamma}(k) = 0$ otherwise. If $\rho(a) = \max(a, 0)$ then $\gamma(\alpha) = \max(\cos \alpha, 0)$ and a direct calculation of Fourier integrals gives

$$\widehat{\gamma}(k) = \begin{cases} \frac{-(i)^k}{\pi(k-1)(k+1)} & \text{if } k \text{ is even} \\ \frac{1}{4} & \text{if } k = \pm 1 \\ 0 & \text{if } |k| > 1 \text{ is odd} \end{cases} . \quad (12)$$

One can verify that any real homogeneous operator can be written $\rho(a) = \alpha \max(a, 0) + \beta a$ so $\widehat{\gamma}(k) = 0$ when $|k| > 1$ is odd. If $\rho(a) = |a|$ then $\gamma(\alpha) = |\cos \alpha|$ and hence

$$\widehat{\gamma}(k) = \begin{cases} \frac{-2(i)^k}{\pi(k-1)(k+1)} & \text{if } k \text{ is even} \\ 0 & \text{if } k \text{ is odd} \end{cases} . \quad (13)$$

Because the absolute value is even and thus loses sign information, we have $\widehat{\gamma}(1) = \widehat{\gamma}(-1) = 0$. One may generalize the calculation of convolutional network coefficients by the formula (7) with any 2π periodic phase transformation $\gamma(\alpha)$. In this case, $\widehat{\gamma}(k)$ may be chosen to be non-zero for odd frequencies $|k| > 1$.

The phase harmonic $[x \star \psi_\lambda(u)]^k$ multiplies the phase $\varphi(x \star \psi_\lambda(u))$ by k . It thus multiplies by k the derivatives of the phase, which correspond to the analytic instantaneous frequencies [9], but it does not affect the energy distribution of the modulus along u . This can be interpreted as a “frequency transposition” similar to a musical transposition. For example, shifting a musical score by one octave multiplies by two the “frequencies” of all musical notes, but it does not change the tempo and the melody. The Fourier support of $x \star \psi_\lambda$ is included in the Fourier support of $\widehat{\psi}_\lambda$ centered at λ . In a first approximation, the Fourier transform of $[x \star \psi_\lambda]^k$ is non negligible over a domain centered in $k\lambda$ whose width is approximatively k times the support width of $\widehat{\psi}_\lambda$. This is expressed by the following proposition, under restrictive hypotheses. A ball in \mathbb{R}^d is written $B(c, r) = \{u \in \mathbb{R}^d : |u - c| \leq r\}$.

Proposition 2.2 *If $|x \star \psi_\lambda(u)|$ and $e^{\varphi(x \star \psi_\lambda(u))}$ have a Fourier transform respectively supported in $B(0, \Delta)$ and $B(\lambda, \Delta)$ then $[x \star \psi_\lambda]^k$ has a Fourier transform supported in $B(k\lambda, (|k| + 1)\Delta)$.*

Proof: Since $[x \star \psi_\lambda]^k = |x \star \psi_\lambda| (e^{i\varphi(x \star \psi_\lambda(u))})^k$ in the Fourier domain it is the convolution of the Fourier transform of $|x \star \psi_\lambda|$ and k successive convolutions of the Fourier transform of $e^{i\varphi(x \star \psi_\lambda(u))}$. The Fourier support of $[x \star \psi_\lambda]^k$ can be derived from the Fourier supports of $|x \star \psi_\lambda|$ and $e^{i\varphi(x \star \psi_\lambda(u))}$ because the convolutions of two functions included in $B(c, r)$ and in $B(c', r')$ is a function included in $B(c + c', r + r')$. \square .

If $\widehat{\psi}_\lambda$ is supported in $B(\lambda, \Delta)$ then $x \star \psi_\lambda$ has a Fourier transform supported in $B(\lambda, \Delta)$ but in general $|x \star \psi_\lambda|$ and $e^{i\varphi(x \star \psi_\lambda(u))}$ do not have a Fourier transform of compact support. Indeed, $|x \star \psi_\lambda|$ may be singular if $x \star \psi_\lambda(u)$ has a zero-crossing, which produces a Fourier transform with a slow asymptotic decay. The hypotheses of this proposition are thus very restrictive. For wavelet filters, Section 4.3 shows numerically that the Fourier transform of $[x \star \psi_\lambda]^k$ is essentially concentrated over a frequency domain which is a dilation by k of the support of $\widehat{\psi}_\lambda$.

2.3 Phase Filtering

Deep neural networks compute linear combinations of rectified coefficients $\rho(x \star \psi_k^r(u))$ along the channel index k . It amounts to combine $Ux(u, \alpha, \lambda)$ along α and λ . In this section we study convolutions along α and prove that they can considerably improve the phase transformation selectivity.

The circular convolution of 2π periodic functions is written

$$a \circledast b(\alpha) = \int_{[0, 2\pi]} a(\beta) b(\alpha - \beta) d\beta.$$

A convolution of $Ux(u, \alpha, \lambda)$ along α by a 2π periodic g gives

$$Ux(u, ., \lambda) \circledast g(\alpha) = |x \star \psi_\lambda(u)| \gamma_g(\varphi(x \star \psi_\lambda(u)) + \alpha), \quad (14)$$

where the phase transformation is now

$$\gamma_g = \gamma \star g \text{ and hence } \widehat{\gamma}_g(k) = \widehat{\gamma}(k) \widehat{g}(k).$$

The following theorem proves that a rectifier and an absolute value may become highly selective after such a filtering.

Theorem 2.1 *If $\gamma(\alpha) = \max(\cos \alpha, 0)$ or $\gamma(\alpha) = |\cos \alpha|$ then for any $\epsilon > 0$ there exists a bounded filter g such that γ_g is differentiable, π periodic, supported in $[-\epsilon, \epsilon]$ modulo π , with $\int_0^{2\pi} \gamma_g(\alpha) d\alpha = 2$, and*

$$\lim_{\epsilon \rightarrow 0} \gamma_g(\alpha) = \delta(\alpha \bmod \pi). \quad (15)$$

Proof: We show that we can define g so that $\gamma_g = \gamma \star g$ is a π periodic cubic box spline supported in $[-\epsilon, \epsilon]$ with $\widehat{\gamma}_g(0) = \int_0^{2\pi} \gamma_g(\alpha) d\alpha = 2$. One can verify that the Fourier transform of this box spline is

$$\widehat{\gamma}_g(k) = \begin{cases} 2 & \text{if } k = 0 \\ 2 \sin^4(k\epsilon/4) (k\epsilon/4)^{-4} & \text{if } k \neq 0 \text{ is even} \\ 0 & \text{if } k \text{ is odd.} \end{cases} \quad (16)$$

For a linear rectifier and an absolute value, $\widehat{\gamma}(k)$ is non-zero when k is even. Since $\widehat{\gamma}_g = \widehat{\gamma} \widehat{g}$ we obtain (16) by defining $\widehat{g}(k) = 0$ if k is odd and $\widehat{g}(k) = \widehat{\gamma}_g(k)/\widehat{\gamma}(k)$ if k is even. We prove that $g(\alpha)$ is bounded by verifying that $\sum_k |\widehat{g}(k)| < \infty$ because $|\widehat{g}(k)| = O(|k|^{-2})$.

The restrictions of γ_g to $[-\pi/2, \pi/2]$ and $[\pi/2, 3\pi/2]$ are bounded functions of integrals equal to 1. Their supports are respectively $[-\epsilon, \epsilon]$ and $[\pi - \epsilon, \pi + \epsilon]$. When ϵ goes to 0 the restrictions of γ_g to $[-\pi/2, \pi/2]$ and $[\pi/2, 3\pi/2]$ thus converge $\delta(\alpha)$ and $\delta(\alpha - \pi)$, which proves (15). \square

This theorem proves that for a linear rectifier or an absolute value, one can improve arbitrarily the phase selectivity through convolutions along angles. This is not true if $\rho(a) = a$. The theorem proof specifies a possible choice for the filters g , and (15) proves that

$$\lim_{\epsilon \rightarrow 0} Ux(u, ., \lambda) \star g(\alpha) = |x \star \psi_\lambda(u)| \delta((\varphi(x \star \psi_\lambda(u)) + \alpha) \bmod \pi). \quad (17)$$

The resulting convolutional network coefficients separate coefficients $x \star \psi_\lambda(u)$ depending upon their exact phase value modulo π . The sign discrimination can be obtained with a linear rectifier as opposed to an absolute value. In the following we shall thus concentrate on linear rectifiers.

2.4 Bi-Lipschitz Phase Harmonics

As opposed to a polynomial exponents z^k used in complex Laurent series expansions, a phase harmonics $[z]^k$ computes an exponent of the phase while preserving the modulus. As a result, we prove that Γ is bi-lipschitz, which is not true for polynomial exponents $k \neq 1$. We derive that neural network operators U are also bi-Lipschitz when computed with appropriate filters.

For any 2π periodic $g(\alpha)$, we write

$$\|g\|^2 = \frac{1}{2\pi} \int_0^{2\pi} |g(\alpha)|^2 d\alpha = \sum_{k \in \mathbb{Z}} |\widehat{g}(k)|^2.$$

Theorem 2.2 For any $(z, z') \in \mathbb{C}^2$

$$\sqrt{2} |\hat{\gamma}(1)| |z - z'| \leq \|\Gamma z - \Gamma z'\| \leq \kappa |z - z'| \quad (18)$$

with

$$\kappa^2 = \frac{1}{4\pi^2} \left(\int_0^{2\pi} \gamma(\alpha) d\alpha \right)^2 + \frac{1}{2\pi} \int_0^{2\pi} |\gamma'(\alpha)|^2 d\alpha, \quad (19)$$

and

$$\|\Gamma z\| = \|\gamma\| |z|. \quad (20)$$

For a linear rectifier, $\|\gamma\| = 1/2$, $\hat{\gamma}(1) = 1/4$ and $\kappa = \sqrt{1/4 + 1/\pi^2}$.

Proof: Since $\hat{\Gamma}z(k) = \hat{\gamma}(k) [z]^k$, we first prove (20) by observing that

$$\|\Gamma z\|^2 = \sum_{k=-\infty}^{+\infty} |\hat{\gamma}(k)|^2 |[z]^k|^2 \leq |z|^2 \sum_{k=-\infty}^{+\infty} |\hat{\gamma}(k)|^2 = |z|^2 \|\gamma\|^2.$$

To verify (18), let us compute

$$\|\Gamma z - \Gamma z'\|^2 = \sum_{k=-\infty}^{+\infty} |\hat{\gamma}(k)|^2 |[z]^k - [z']^k|^2. \quad (21)$$

Since $\gamma(\alpha)$ is real, $|\hat{\gamma}(k)| = |\hat{\gamma}(-k)|$. Restricting the sum to $k = \pm 1$ gives the lower bound

$$2 |\hat{\gamma}(1)|^2 |z - z'|^2 \leq \|\Gamma z - \Gamma z'\|^2.$$

The upper-bound of (18) is obtained by proving that for any $(z, z') \in \mathbb{C}^2$

$$|[z]^k - [z']^k| \leq \max(1, |k|) |z - z'|. \quad (22)$$

This is verified if $k = 0$ because

$$|[z]^k - [z']^k| = ||z| - |z'|| \leq |z - z'|.$$

For $k \neq 0$ and $\epsilon = \varphi(z') - \varphi(z)$, let us define

$$\begin{aligned} f(|z|, |z'|, \epsilon) &= \frac{|[z]^k - [z']^k|^2}{|z - z'|^2} = \frac{||z| - |z'| e^{ik\epsilon}|^2}{||z| - |z'| e^{i\epsilon}|^2} \\ &= \frac{||z|^2 + |z'|^2 - 2|z||z'| \cos(k\epsilon)|}{||z|^2 + |z'|^2 - 2|z||z'| \cos(\epsilon)|} \end{aligned}$$

We shall prove that

$$\sup_{|z|,|z'|,\epsilon} f(|z|,|z'|,\epsilon) = |k|^2,$$

which implies (22). This is done by verifying that for $|z|$ and $|z'|$ fixed, the maximum of f is reached when ϵ tends to 0, and when ϵ tends to zero $f(\epsilon, |z|, |z'|)$ is maximized when $|z| = |z'|$, with a supremum equal to $|k|^2$.

We obtain the upper bound inequality of (18) by inserting (22) in (21) with

$$\kappa^2 = |\widehat{\gamma}(0)|^2 + \sum_{k \in \mathbb{Z}} k^2 |\widehat{\gamma}(k)|^2, \quad (23)$$

Since $\widehat{\gamma}(0) = 1/2\pi \int_0^{2\pi} \gamma(\alpha) d\alpha$ and the Fourier transform of $\gamma'(\alpha)$ is $ik\widehat{\gamma}(k)$, applying the Plancherel formula on (23) proves (19). A direct calculation gives the values of $\|\gamma\|$ and κ for a linear rectifier where $\gamma(\alpha) = \max(\cos \alpha, 0)$. \square

The Lipschitz constant κ in (19) is finite if $\gamma(\alpha) = \rho(\cos \alpha)$ has a derivative in $\mathbf{L}^2[0, 2\pi]$ and hence if ρ has a bounded derivative. For a linear rectifier the lower and upper Lipschitz constants are respectively about 0.35 and 0.69 and thus within a factor 2.

The following theorem gives a condition on the filters $\{\psi_\lambda\}_{\lambda \in \Lambda}$ so that W is bi-Lipschitz and $U = \Gamma W$ is also bi-Lipschitz. We write

$$\|Ux\|^2 = \frac{1}{2\pi} \sum_{\lambda \in \Lambda} \int_0^{2\pi} \int_{\mathbb{R}^d} |Ux(u, \alpha, \lambda)|^2 du d\alpha.$$

Theorem 2.3 *If there exists $\eta < 1$ such that for almost all $\omega \in \mathbb{R}^d$*

$$(1 - \eta)^2 \leq \frac{1}{2} \sum_{\lambda \in \Lambda} \left(|\widehat{\psi}_\lambda(\omega)|^2 + |\widehat{\psi}_\lambda(-\omega)|^2 \right) \leq (1 + \eta)^2 \quad (24)$$

then for all $x \in \mathbf{L}^2(\mathbb{R}^d)$ real

$$\|\gamma\| (1 - \eta) \|x\| \leq \|Ux\| \leq \|\gamma\| (1 + \eta) \|x\| \quad (25)$$

and for all $(x, x') \in \mathbf{L}^2(\mathbb{R}^d)^2$ real

$$\sqrt{2} |\widehat{\gamma}(1)| (1 - \eta) \|x - x'\| \leq \|Ux - Ux'\| \leq \kappa (1 + \eta) \|x - x'\|. \quad (26)$$

Proof: Let us first show that (24) implies that

$$(1 - \eta)^2 \|x - x'\|^2 \leq \|Wx - Wx'\|^2 \leq (1 + \eta)^2 \|x - x'\|^2. \quad (27)$$

Since W is linear, it is equivalent to prove it for $x' = 0$. Observe that

$$\|Wx\|^2 = \sum_{\lambda \in \Lambda} \|x \star \psi_\lambda\|^2 = \frac{1}{(2\pi)^d} \sum_{\lambda \in \Lambda} \int |\widehat{x}(\omega)|^2 |\widehat{\psi}_\lambda(\omega)|^2 d\omega.$$

Since x is real, $|\widehat{x}(\omega)| = |\widehat{x}(-\omega)|$. Inverting the sum and the integral and inserting (24) in this equation proves (27) for $x' = 0$.

Since $U = \Gamma W$, (27) together with (20) proves (25), and (27) together with (18) proves (26). \square

This theorem proves that a one-layer convolution network operator U is invertible and Lipschitz stable.

3 Integral and Correlation Invariants

3.1 Phase Selectivity of Integrals and Correlations

We define a translation invariant representation from a one-layer neural network, by integrating the output network coefficients and by computing their correlations along the spatial variable u . Such correlation coefficients are used by Ustyuzhaninov et. al. [15] to generate stationary image textures from random filters. We prove that filtering the phase can provide integrals and correlations over domains where the phase remains constant.

First order translation invariant coefficients are computed by integrating convolutional network coefficients along u :

$$Ix(\alpha, \lambda) = \int Ux(u, \alpha, \lambda) du \quad (28)$$

$$= \int |x \star \psi_\lambda(u)| \gamma(\varphi(x \star \psi_\lambda(u)) + \alpha) du. \quad (29)$$

The phase selectivity of γ can be modified by a convolution along α :

$$Ix(., \lambda) \circledast g(\alpha) = \int |x \star \psi_\lambda(u)| \gamma_g(\varphi(x \star \psi_\lambda(u)) + \alpha) du \quad (30)$$

with $\gamma_g = \gamma \circledast g$. For the filters defined by Theorem 2.1, γ_g restricts the integral to sets of points u where the phase $\varphi(x \star \psi_{\lambda'}(u))$ is in $[-\alpha - \epsilon, -\alpha + \epsilon]$ modulo π . When ϵ goes to zero, it proves that Ix specifies the integral $|x \star \psi_{\lambda}(u)|$ over all lines of constant phase α modulo π . For wavelet filters and images, Section 4 shows that lines of constant phase define the geometry of multiscale edges.

Second order invariants are spatial correlations of neural network coefficients:

$$Cx(\alpha, \alpha', \lambda, \lambda') = \int Ux(u, \alpha, \lambda) Ux(u, \alpha', \lambda') du \quad (31)$$

$$= \int |x \star \psi_{\lambda}(u)| |x \star \psi_{\lambda'}(u)| \gamma(\varphi(x \star \psi_{\lambda}(u)) + \alpha) \gamma(\varphi(x \star \psi_{\lambda'}(u)) + \alpha') du. \quad (32)$$

The convolution with a separable filter $G(\alpha, \alpha') = g(\alpha) g(\alpha')$ replaces γ by $\gamma_g = \gamma \circledast g$. For the filters of Theorem 2.1, it correlates $|x \star \psi_{\lambda}(u)|$ and $|x \star \psi_{\lambda'}(u)|$ over points u where $\varphi(x \star \psi_{\lambda}(u)) \in [-\alpha - \epsilon, -\alpha + \epsilon]$ and $\varphi(x \star \psi_{\lambda'}(u)) \in [-\alpha' - \epsilon, -\alpha' + \epsilon]$ modulo π . In the limit of ϵ going to zero, the integral is thus restricted to intersections of lines of constant phases $-\alpha$ and $-\alpha'$. For wavelet filters, these lines of constant phase follow the geometry of structures appearing at different scales. Correlation coefficients capture the modification of this geometry across scale.

3.2 Lipschitz Phase Harmonic Integrals and Correlations

We compute the Fourier transform along phases of one-layer networks integrals and correlations. It defines phase harmonics integrals and correlations. We study their properties and prove that they are Lipschitz continuous to additive perturbations of the input signal.

Since $Ix(\alpha, \lambda) = \int Ux(u, \alpha, \lambda) du$, equation (11) implies that its Fourier transform along α is

$$\widehat{Ix}(k, \lambda) = \int \widehat{U}x(u, k, \lambda) du = \widehat{\gamma}(k) \int [x \star \psi_{\lambda}(u)]^k du. \quad (33)$$

For $k = 0$, $[x \star \psi_{\lambda}]^0 = |x \star \psi_{\lambda}|$ so it gives \mathbf{L}^1 norms:

$$\widehat{Ix}(0, \lambda) = \widehat{\gamma}(0) \|x \star \psi_{\lambda}\|_1.$$

For $k = 1$, $[x \star \psi_\lambda]^1 = x \star \psi_\lambda$ so

$$\widehat{Ix}(1, \lambda) = \widehat{\gamma}(1) \int \psi_\lambda(u) du \int x(u) du .$$

If $\int \psi_\lambda(u) du = 0$ then $\widehat{Ix}(1, \lambda) = 0$. Section 4.3 shows that for wavelet filters, integral coefficients have small amplitudes for $k \geq 1$. The dominating invariants are \mathbf{L}^1 norms $\|x \star \psi_\lambda\|_1$.

Similarly, the Fourier transform of $Cx(\alpha, \alpha', \lambda, \lambda')$ along α and α' defines correlations between phase harmonics

$$\begin{aligned} \widehat{Cx}(k, k', \lambda, \lambda') &= \int \widehat{Ux}(u, k, \lambda) \widehat{U}(u, k', \lambda')^* du \\ &= \widehat{\gamma}(k) \widehat{\gamma}(k')^* \int [x \star \psi_\lambda(u)]^k [x \star \psi_{\lambda'}(u)]^{-k'} du. \end{aligned} \quad (34)$$

Diagonal coefficients are proportional to \mathbf{L}^2 norms

$$\widehat{Cx}(k, k, \lambda, \lambda) = |\widehat{\gamma}(k)|^2 \|x \star \psi_\lambda\|_2^2.$$

When the ψ_λ are band-pass filters over different frequency bands then the harmonic correlation \widehat{Cx} is sparse. Indeed, the Plancherel formula applied to (34) proves that $\widehat{Cx}(k, k', \lambda, \lambda')$ is nearly zero if the Fourier transforms of $[x \star \psi_\lambda(u)]^k$ and $[x \star \psi_{\lambda'}(u)]^{-k'}$ are concentrated over frequency domains which do not intersect. Since the center frequencies are approximatively $k\lambda$ and $k'\lambda'$, the coefficients are negligible when $|k\lambda - k'\lambda'|$ is too large. The non-negligible coefficients for $k\lambda \approx k'\lambda'$ provide important non-linear correlations between different frequency bands.

We now prove that the invariant integral Ix and correlation Cx are also Lipschitz continuous for appropriate norms. The same Lipschitz bounds apply to \widehat{Ix} and \widehat{Cx} since they are computed by applying a Fourier transform on Ix and Cx , and the Fourier transform is a unitary operator which does not modify these norms. To establish the result for $Ix(u, \alpha, \lambda) = \int Ux(u, \alpha, \lambda) du$, we need to normalize the integral by the size of the integration domain so that it becomes an average. We shall thus suppose that x has a compact support in $[0, K]^d$ and that all convolutions are computed as periodic convolutions over this domain so that $x \star \psi_\lambda \in \mathbf{L}^2([0, K]^d)$.

This normalization is not necessary for the correlation matrix. For any $x \in \mathbf{L}^2(\mathbb{R}^d)$, the matrix $Cx(\alpha, \alpha', \lambda, \lambda')$ is the kernel of a positive symmetric

operator, whose sup operator norm is computed by applying Cx to vectors $w(\alpha, \lambda)$:

$$\|Cx\|_\infty = \sup_w \frac{\|Cx w\|}{\|w\|} \quad \text{with} \quad \|w\|^2 = \frac{1}{2\pi} \sum_{\lambda \in \Lambda} \int_0^{2\pi} |w(\alpha, \lambda)|^2 d\alpha .$$

The following theorem computes Lipschitz bounds for these norms.

Theorem 3.1 *If the filters ψ_λ satisfy (24) then for all $(x, x') \in \mathbf{L}^2([0, K]^d)^2$*

$$\|Ix - Ix'\| \leq \kappa (1 + \eta) K^{d/2} \|x - x'\| , \quad (35)$$

where κ is defined in (19). For all $x \in \mathbf{L}^2(\mathbb{R}^d)$

$$(1 - \eta)^2 \|\gamma\|^2 \|x\|^2 \leq \text{Trace}(Cx) \leq (1 + \eta)^2 \|\gamma\|^2 \|x\|^2 , \quad (36)$$

and all $(x, x') \in \mathbf{L}^2(\mathbb{R}^d)^2$

$$\|Cx - Cx'\|_\infty \leq 2\kappa^2 (1 + \eta)^2 \|x - x'\| (\|x\| + \|x - x'\|) . \quad (37)$$

Proof: We write the integral Ix in (28) in a vector form $Ix = \int Ux(u, \cdot) du$, which gives

$$\|Ix - Ix'\|^2 = \left\| \int (Ux(u, \cdot) - Ux'(u, \cdot)) du \right\|^2 .$$

If $y \in \mathbf{L}^2([0, K]^d)$ then Cauchy-Schwartz implies

$$\left| \int_{[0, K]^d} y(u) du \right|^2 \leq K^d \int_{[0, K]^d} |y(u)|^2 du .$$

Applied to the vector $Ux(u, \cdot) - Ux'(u, \cdot)$ it gives

$$\|Ix - Ix'\|^2 \leq K^d \int \|Ux(u, \cdot) - Ux'(u, \cdot)\|^2 du .$$

Applying the Lipschitz upper bound (26) proves (35).

The operator Cx is defined in (31) as the autocorrelation of Ux which we write in a vector form $Cx = \int Ux(u, \cdot) Ux(u, \cdot)^t du$, where $Ux(u, \cdot)^t$ is the transpose of $Ux(u, \cdot)$. By writing $Ux' = Ux + (Ux' - Ux)$ we verify that

$$\begin{aligned} Cx' - Cx &= \int \left(Ux(u, \cdot) (Ux'(u, \cdot) - Ux(u, \cdot))^t + (Ux'(u, \cdot) - Ux(u, \cdot)) Ux(u, \cdot)^t \right) du \\ &\quad + \int (Ux'(u, \cdot) - Ux(u, \cdot)) (Ux'(u, \cdot) - Ux(u, \cdot))^t du . \end{aligned} \quad (38)$$

Any operator with kernel $C(a, b) = \int A(u, a) B(u, b) du$ has a sup opertor norm which satisfies

$$\|C\|_\infty \leq \|A\| \|B\| \quad (39)$$

with $\|A\|^2 = \int \sum_a |A(u, a)|^2 du$ and $\|B\|^2 = \int \sum_a |B(u, a)|^2 du$. This is verified with the Cauchy Schwartz inequality by verifying that for any vectors w and w' :

$$|\langle w, Cw' \rangle| \leq \|w\| \|w'\| \|A\| \|B\| .$$

Applying (39) to (38) proves that

$$\|Cx - Cx'\|_\infty \leq \|Ux - Ux'\| (2\|Ux\| + \|Ux - Ux'\|).$$

Since $\|Ux - Ux'\| \leq \kappa(1 + \eta) \|x - x'\|$ and $\|Ux\| \leq \|\gamma\| (1 + \eta) \|x\|$ with $\|\gamma\|^2 \leq \kappa^2$, we derive (37). \square

For any fixed x , Cx is a postive symmetric operator so $\|Cx\|_\infty \leq \text{Trace}(Cx)$. The theorem proves in (36) that Cx is a bounded operator for the sup operator norm, and that it is Lipschitz continuous when x' varies in the neighborhood of x . The theorem results also apply to $\widehat{I}x$ and $\widehat{C}x$, which are computed from Ix and Cx with a unitary Fourier transform.

4 Wavelet Phase Harmonics Correlations

Wavelet filters separate signal variations at multiple scales. They provide invariant signal descriptors which are stable to deformations, and are thus a natural choice to compute convolutional neural network coefficients [10]. Sections 4.1 and 4.2 review the properties of complex analytic wavelet transform and introduce a new bump wavelet. Section 4.3 shows that the resulting phase harmonic coefficients have a sparse correlation matrix.

4.1 Analytic Bump Wavelet for 1D Signals

A one-dimensional wavelet transform is computed by convolutions with dilated wavelets. To define the notion of phase as in Section 2.1, we define a complex analytic wavelet ψ , whose Fourier transform $\widehat{\psi}(\omega)$ is zero at negative frequencies. This section introduces a new analytic bump wavelet, which is used in numerical calculations.

A wavelet transform with Q scales per octave is calculated by dilating ψ by $2^{j/Q}$, where j is an integer:

$$\psi_\lambda(u) = 2^{-j/Q} \psi(2^{-j/Q} u) \text{ and hence } \widehat{\psi}_\lambda(\omega) = \widehat{\psi}(2^{j/Q} \omega) .$$

If ξ is the center frequency of ψ then the center frequency of ψ_λ is

$$\lambda = 2^{-j/Q} \xi .$$

We impose that $\widehat{\psi}(\lambda)$ is real and positive. If the energy of $\widehat{\psi}(\omega)$ is concentrated in an interval centered in ξ of radius $\beta\xi$ then $\widehat{\psi}_\lambda$ is concentrated in an interval centered in λ of radius $\beta\lambda$.

If $\widehat{\psi}_\lambda$ is real valued then the real part of ψ_λ is even and its imaginary part is odd. A real filter of phase α is defined by $\text{Real}(e^{i\alpha}\psi_\lambda)$. The phase α is thus a symmetry parameter which makes the transition from even to odd filters, and which changes filter sign when adding π .

Let 2^J be the maximum scale. Scales larger than 2^J are carried by a low-pass filter ψ_0 centered at the frequency $\lambda = 0$ and dilated by 2^J . We use a Gaussian filter whose Fourier transform is

$$\widehat{\psi}_0(\omega) = \exp\left(-\frac{|\omega|^2}{2\sigma_J^2}\right). \quad (40)$$

We consider an analytic wavelets whose Fourier transform $\widehat{\psi}(\omega)$ is a regular window centered at a frequency $\xi > 0$

$$\widehat{\psi}(\omega) = c w\left(\frac{\omega - \xi}{\xi}\right), \quad (41)$$

where $w(\omega)$ has a support in $[-1, 1]$ so that $\widehat{\psi}(\omega) = 0$ for $\omega \leq 0$. A bump window is an infinitely differentiable approximation of a Gaussian having a compact support in $[-1, 1]$, used in signal processing [6]:

$$w(\omega) = \exp\left(\frac{-|\omega|^2}{1 - |\omega|^2}\right) 1_{[-1,1]}(\omega) . \quad (42)$$

It defines a compact support $\widehat{\psi}(\omega)$ which is \mathbf{C}^∞ . The resulting *bump* wavelet ψ is a Schwartz class \mathbf{C}^∞ analytic function, with a decay faster than any rational function. Since all derivatives of $\widehat{\psi}_\lambda$ vanish at $\omega = 0$, ψ has an infinite number of vanishing moments:

$$\forall k \in \mathbb{N} , \quad \int u^k \psi(u) du = 0 .$$

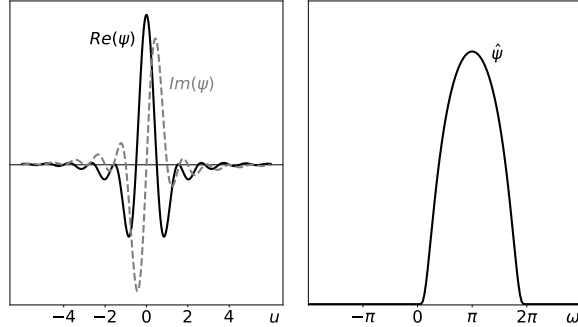


Figure 1: Left: real (full) and imaginary (dashed) parts of a bump wavelet $\psi(u)$ with $Q = 1$. Right: Fourier transform $\hat{\psi}(\omega)$.

Vanishing moments are important so that wavelet coefficients $x \star \psi_\lambda(u)$ are small in domains of u where x is regular [9].

In order to minimize the Littlewood-Paley constant η in (24), the constants in (40) and (41) are chosen to be

$$\sigma_J = 2^{\frac{-0.550}{Q}} 2^{-J+1} \xi \quad \text{and} \quad c = (1.34\sqrt{Q} - 0.05)^{-1}.$$

In numerical applications, we choose $\xi = 0.85\pi$. For these bump wavelets, $\eta = 0.091$ when $Q = 1$ and $\eta \leq 0.035$ when $Q \geq 2$. Figure 1 shows the real and imaginary parts of ψ for $Q = 1$, as well as its Fourier transform.

Figure 2 gives the modulus and the phase of the wavelet transform of a one-dimensional signal, calculated with a bump wavelet, with $Q = 16$ scales per octaves. At fine scales, which correspond to high frequencies λ , large modulus coefficients $|x \star \psi_\lambda(u)|$ are located in the neighborhood of sharp signal transitions. The phase $\varphi(x \star \psi_\lambda(u))$ gives a local symmetry information on the transition of $x \star \psi_\lambda$ at u . Since the real and imaginary parts of ψ_λ are respectively symmetric and antisymmetric, if $\varphi(x \star \psi_\lambda(u)) = 0$ then the variations of $x \star \psi_\lambda(u)$ is locally symmetric in the neighborhood of u and it is antisymmetric if the phase is $\pi/2$. A change of sign adds π to the phase. When the phase is $\pi/2$ modulo π then the real part of $x \star \psi_\lambda(u)$ has a zero-crossing. Zero-crossings of real wavelet transforms have been studied to reconstruct signals and detect the position of sharp transitions [8]. Grossmann et. al. [1] showed that lines of constant phase across scales capture properties of instantaneous frequencies.

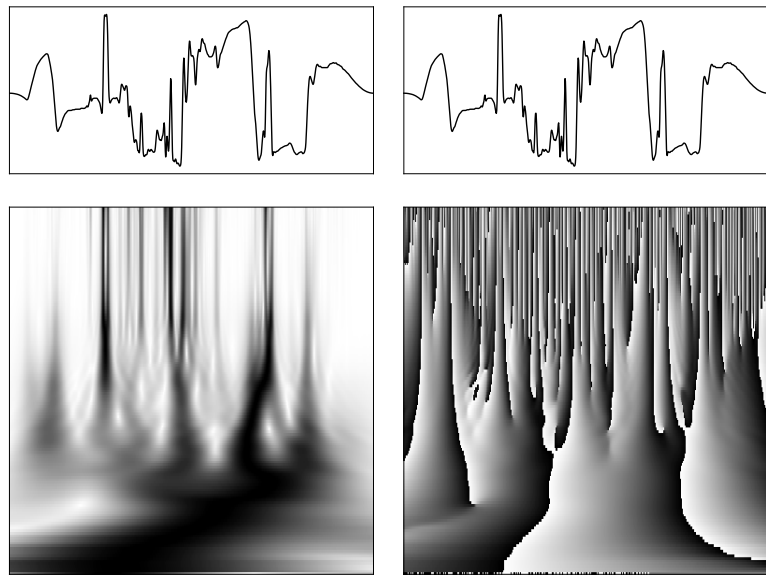


Figure 2: Top: original signal $x(u)$ as a function of u . Left: wavelet transform modulus $|x * \psi_\lambda(u)|$ with $Q = 16$ scales per octave. White and black points correspond respectively to small and large amplitudes. The log frequency $\log_2 \lambda$ increases along the vertical axis, from bottom to top. Right: complex phase $\varphi(x * \psi_\lambda(u))$ as a function of u and $\log_2 \lambda$.

4.2 Complex Steerable Bump Wavelets for Images

In two dimensions, we define wavelets by dilating and rotating a complex analytic wavelet $\psi(u)$ for $u \in \mathbb{R}^2$. Its Fourier transform $\widehat{\psi}(\omega)$ has a support included in the right half plane of \mathbb{R}^2 . This wavelet is rotated by several angles θ in \mathbb{R}^2 with r_θ and dilated at dyadic scales 2^j :

$$\psi_\lambda(u) = 2^{-2j} \psi(2^{-j} r_{-\theta} u) \text{ and hence } \widehat{\psi}_\lambda(\omega) = \widehat{\psi}(2^j r_\theta \omega) .$$

We use L angles $\theta = \pi\ell/L$ for $0 \leq \ell < L$. If ξ is the center frequency of ψ then the center frequency of ψ_λ is

$$\lambda = 2^{-j} r_{-\theta} \xi .$$

Wavelets are computed up to a maximum scale 2^J . Scales larger than 2^J are carried by a low-pass filter ψ_0 centered at the frequency $\lambda = 0$ and dilated by 2^J . As in one dimension, we use a Gaussian filter whose Fourier transform is

$$\widehat{\psi}_0(\omega) = \exp\left(-\frac{|\omega|^2}{2\sigma_J^2}\right) . \quad (43)$$

Let us represent frequencies in polar coordinates $\omega = |\omega|(\cos\phi, \sin\phi)$. Steerable wavelet introduced by Simoncelli et. al [13] have a center frequency $\xi = (\xi_0, 0)$ with L rotation angles, and a Fourier transform $\widehat{\psi}(\omega)$ which can be written:

$$\widehat{\psi}(\omega) = c w\left(\frac{|\omega| - \xi_0}{\xi_0}\right) \cos^{L-1}(\phi) 1_{|\phi| < \frac{\pi}{2}} . \quad (44)$$

Different wavelets are obtained by modifying the window w [14]. Steerable bump wavelets are computed with the one-dimensional bump window w in (42). Since $\widehat{\psi}(\omega)$ has L bounded derivatives and a compact support, the resulting complex wavelet $\psi(u)$ is a \mathbf{C}^∞ function and $|\psi(u)| = O((1+|u|)^{-L})$. All partial derivatives of $\widehat{\psi}(\omega)$ are zero at $\omega = 0$ so ψ has an infinite number of vanishing moments

$$\forall (k_1, k_2) \in \mathbb{Z}^2 , \quad \int_{\mathbb{R}^2} u_1^{k_1} u_2^{k_2} \psi(u_1, u_2) du_1 du_2 = 0 .$$

To minimize the Littlewood-Paley constant η in (24), the constants in (43) and (44) are chosen to be

$$\sigma_J = 2^{-0.550} 2^{-J+1} \xi \quad \text{and} \quad c = 1.29^{-1} 2^{L-1} \frac{(L-1)!}{\sqrt{L[2(L-1)]!}}$$

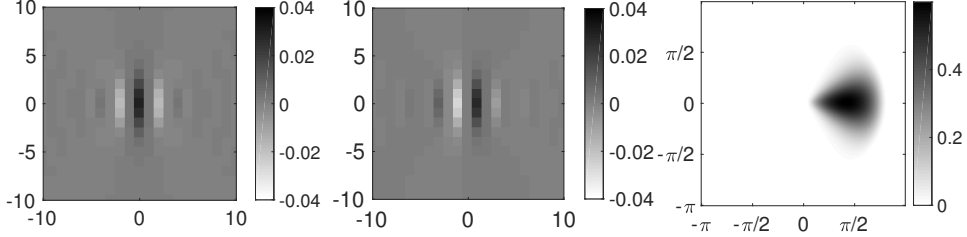


Figure 3: (a): Real part of the two-dimensional bump wavelet $\psi(u)$ with $L = 8$. (b) Imaginary part of $\psi(u)$. (c): Fourier transform $\widehat{\psi}(\omega)$.

In numerical applications, we choose $\xi = 0.85\pi$ and $L \geq 4$. One can verify that the Littlewood-Paley constant is $\eta = 0.091$ as for the one-dimensional wavelet (42) and does not depend upon L . Figure 3 shows the real and imaginary parts of ψ as well as its Fourier transform for $L = 8$ angles.

Figure 4 shows the phase and modulus of the wavelet transform of an image, calculated with bump steerable wavelets at angles $\theta = 0$ and $\theta = \pi/2$ and scales $2^j = 2, 4, 8$. Large modulus coefficients $|x * \psi_\lambda(u)|$ are along edges and sharp transitions. The decay of these modulus values when $|\lambda|$ increases depends upon the Lipschitz regularity of x at u [5]. The phase $\varphi(x * \psi_\lambda(u))$ measures the local symmetry of the variations of $x * \psi_\lambda(u)$ when u moves along the direction of θ . This symmetry is typically preserved along a contours which is why lines of constant phase follow the geometry of contours. This observation is at the basis of many edge detection algorithms [9]. The phase evolution across scales specifies the edge profile.

4.3 Sparse Wavelet Phase Harmonic Correlations

We shall see that the wavelet correlation matrix $Cx(\alpha, \alpha', \lambda, \lambda')$ is a full matrix whereas its Fourier phase harmonic representation $\widehat{Cx}(k, k', \lambda, \lambda')$ is sparse. The same properties applies to $Ix(\alpha, \lambda)$ compared to $\widehat{Ix}(k, \lambda)$.

The phase correlation matrix of rectified wavelet coefficients is

$$Cx(\alpha, \alpha', \lambda, \lambda') = \int \rho(x * \text{Real}(e^{i\alpha}\psi_\lambda)(u)) \rho(x * \text{Real}(e^{i\alpha'}\psi_{\lambda'})(u)) du. \quad (45)$$

If $\lambda = \lambda'$ then it is a function of $\alpha - \alpha'$. For a fixed (λ, λ') it is a full matrix which has a regular 2π periodic oscillation as a function of α and α' . This is shown in the Figure 6 for a one-dimensional signal and an image.

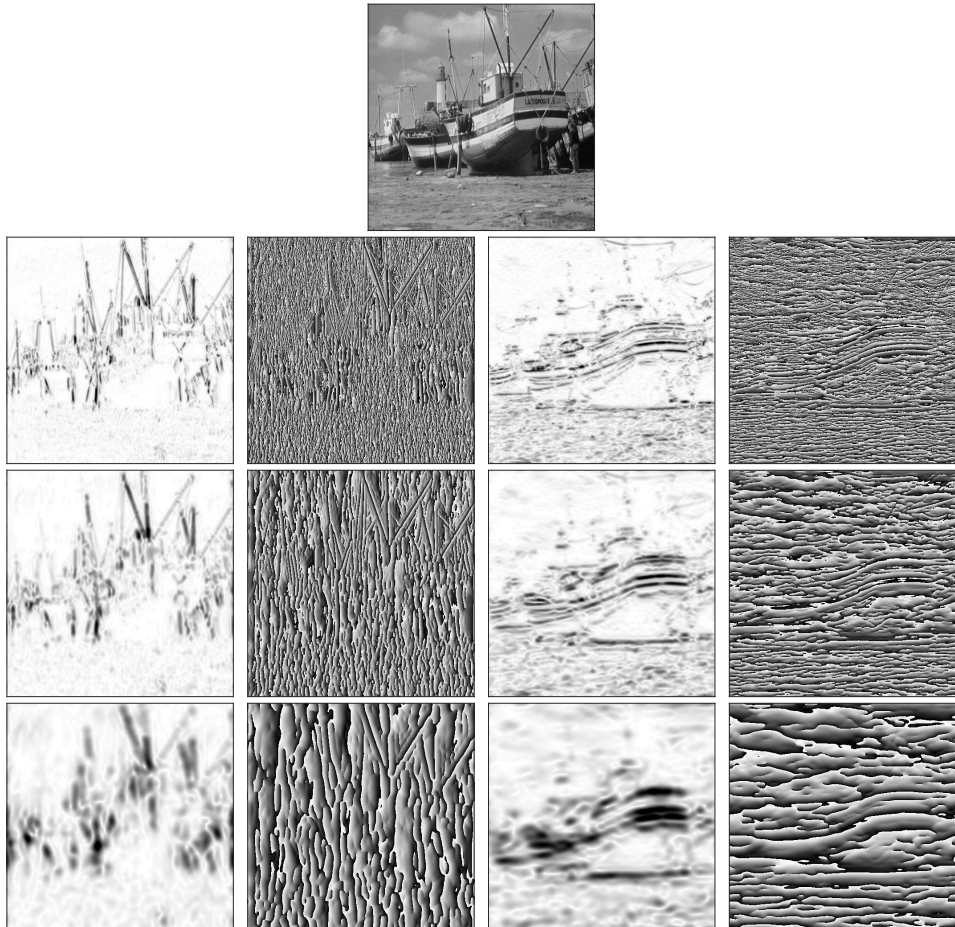


Figure 4: Top: original image. The first column $|x \star \psi_\lambda(u)|$ at scales $2^j = 2, 4, 8$ from top to bottom, for a direction $\theta = 0$. The third row displays modulus coefficients in the perpendicular direction $\theta = \pi/2$. Small and large coefficients are displayed in white and black respectively. The phase images $\varphi(x \star \psi_\lambda)$ are shown in the second and third rows.

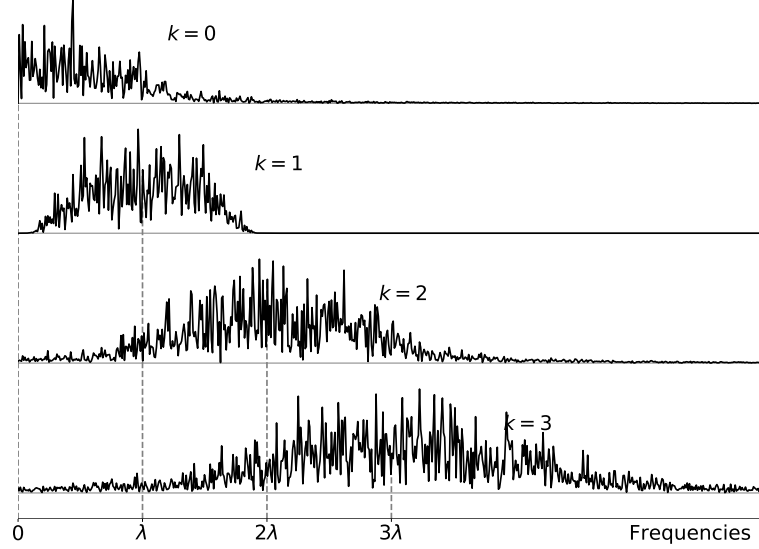


Figure 5: Modulus of the Fourier transform of $[x * \psi_\lambda]^k$, for a realization x of a Gaussian white noise, as a function of frequencies. The wavelet center frequency λ is fixed and k increases from top to bottom.

The representation of the correlation in a Fourier basis along the phase is a matrix of phase harmonic coefficients:

$$\widehat{C}x(k, k', \lambda, \lambda') = \widehat{\gamma}(k) \widehat{\gamma}(k')^* \int [x * \psi_\lambda(u)]^k [x * \psi_{\lambda'}(u)]^{-k'} du. \quad (46)$$

For $k = 1$, $x * \psi_\lambda$ has a Fourier transform centered at the frequency λ and a bandwidth equal to the bandwidth of $\widehat{\psi}_\lambda$ and hence proportional to $|\lambda|$. The Fourier transform of $[x * \psi_\lambda]^k$ is approximately dilated by k . It is centered at $k\lambda$, and its bandwidth is proportional to $k|\lambda|$ for $k \geq 1$ and to $|\lambda|$ for $k = 0$. This is numerically illustrated by Figure 5 which displays the Fourier transform of $[x * \psi_\lambda]^k$ depending upon k , when x which is a realization of a Gaussian white noise.

The Plancherel formula applied to (46) proves that $\widehat{C}x(k, k', \lambda, \lambda')$ is zero if the support of the Fourier transform of $[x * \psi_\lambda]^k$ and of $[x * \psi_{\lambda'}]^{k'}$ do not overlap. The Fourier transform of $[x * \psi_\lambda]^k$ has most of its energy concentrated in a ball centered in $k\lambda$ of radius $\beta|\lambda|$. It results that $\widehat{C}x(k, k', \lambda, \lambda')$ is non-negligible if the distance between the center frequencies $k\lambda$ and $k\lambda'$

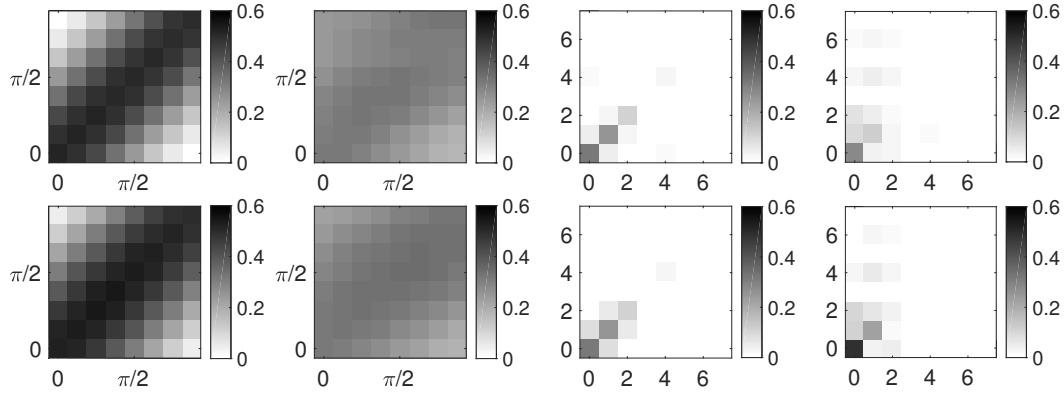


Figure 6: Correlations Cx and \widehat{Cx} for the one-dimensional signal of Figure 2 on the first row, and for the image of Figure 4 on the second row. The images of columns 1 and 2 display $|Cx(\alpha, \alpha', \lambda, \lambda')|^{1/2}/(\|x \star \psi_\lambda\| \|x \star \psi_{\lambda'}\|)^{1/2}$ for 8^2 values of $(\alpha, \alpha') \in [0, \pi]^2$, for a particular $\lambda' = \lambda$ in the first column and $\lambda' = 4\lambda$ in the second column. The images of columns 3 and 4 display $|\widehat{Cx}(k, k', \lambda, \lambda')|^{1/2}/(\|x \star \psi_\lambda\| \|x \star \psi_{\lambda'}\|)^{1/2}$ for $(k, k') \in [0, 7]^2$ and the same $\lambda' = \lambda$ (first column) and $\lambda' = 4\lambda$ (second column).

satisfy

$$|k\lambda - k'\lambda'| \leq \beta (k|\lambda| + k'|\lambda'|). \quad (47)$$

The radii $k\beta|\lambda|$ and $k'\beta|\lambda'|$ must be replaced respectively by $\beta|\lambda|$ or $\beta|\lambda'|$ if $k = 0$ or $k' = 0$. When (k, k') varies for (λ, λ') fixed, (47) defines a band of non-negligible coefficients centered at $k\lambda = k'\lambda'$. Beyond this band, $\hat{Cx}(k, k', \lambda, \lambda')$ is nearly zero, which yields a sparse matrix. This property is illustrated by Figure 6. for the one-dimensional signal of Figure 2 and the image of Figure 4. The first two columns of Figure 6 show that $Cx(\alpha, \alpha', \lambda, \lambda')$ for $\lambda = \lambda'$ and $\lambda' = 4\lambda$ are full matrices whereas their Fourier transforms $\hat{Cx}(k, k', \lambda, \lambda')$ are sparse.

Let us now show that the integral invariants are also highly sparsified in the phase harmonic Fourier domain with a single large coefficient for $k = 0$:

$$\hat{Ix}(k, \lambda) = \hat{\gamma}(k) \int [x \star \psi_\lambda(u)]^k du \ll \hat{Ix}(0, \lambda) = \hat{\gamma}(0) \int |x \star \psi_\lambda(u)| du.$$

The integral of $[x \star \psi_\lambda]^k$ is the value of its Fourier transform at the zero frequency. For $k = 1$, $\hat{Ix}(1, \lambda) = 0$ because $\hat{\psi}_\lambda(0) = 0$. For $k > 1$ the support of $[x \star \psi_\lambda]^k$ is approximatively a dilation of the support of $x \star \psi_\lambda$ so its Fourier transform remains negligible at $\omega = 0$, as illustrated by Figure 5 for a Gaussian white noise. This is verified numerically over one and two-dimensional signals for bump wavelets by evaluating

$$\epsilon = \max_{k>0, \lambda} \frac{|\hat{Ix}(k, \lambda)|}{\hat{Ix}(0, \lambda)}.$$

The numerical values are $\epsilon = 0.017$ for the one-dimensional signal of Figure 2 and $\epsilon = 0.019$ for the image in Figure 4. The fact that integrals $\hat{I}(k, \lambda)$ are essentially non-zero for $k = 0$ means that $I(\alpha, \lambda)$ remains nearly constant when α varies.

5 Reconstruction from Wavelet Phase Harmonic Invariants

Correlations of one layer neural network coefficients are translation invariant. They are studied in [15] to generates stationary image textures having similar perceptual properties as an original texture x . The image texture synthesis

algorithm of Reconstructions of signals x from a translation invariant representation has been widely studied for the Fourier transform modulus $|\widehat{x}|$. For one and two dimensional signals, the reconstruction is possible if x has a compact support but it is generally unstable [2]. This section shows that one can reconstruct close approximations of large classes of signals x , up to a global translation, from integrals and correlations of wavelet phase harmonic coefficients.

5.1 Gradient Descent Reconstructions

Section 4.3 shows that integrals $\widehat{I}x$ and correlations $\widehat{C}x$ of phase harmonic coefficients are sparse. We compute approximations \tilde{x} of x from small fractions of non-negligible coefficients.

We denote by $\|A\|_F$ the Frobenius norm of a matrix A and by V^{t*} the complex conjugate transpose of a vector V . We want to recover x given $\widehat{I}x$ and $\widehat{C}x$. This is done by finding \tilde{x} which minimizes the Frobenius norm of a symmetric error matrix:

$$\mathcal{E}(\tilde{x}) = \|\widehat{C}\tilde{x} - \widehat{C}x - \widehat{I}x(\widehat{I}\tilde{x} - \widehat{I}x)^{t*} - (\widehat{I}\tilde{x} - \widehat{I}x)Ix^{t*}\|_F^2.$$

We consider that $x(u)$ is defined over a support $u \in [0, 1]^d$ and is uniformly sampled over N^d points. Integrals are thus approximated by a normalized Riemann sum

$$\widehat{I}x(k, \lambda) = N^{-d} \sum_u [x \star \psi_\lambda(u)]^k$$

and

$$\widehat{C}x(k, k', \lambda, \lambda') = N^{-d} \sum_u [x \star \psi_\lambda(u)]^k [x \star \psi_{\lambda'}(u)]^{-k'}.$$

The gradient descent is initialized by taking \tilde{x}_0 to be a realization of a Gaussian white noise. The gradient descent computes \tilde{x}_{n+1} from \tilde{x}_n with a gradient step on $\mathcal{E}(\tilde{x}_n)$.

We use an unconstrained gradient descent implemented in standard software packages to reconstruct the original image. The algorithm stops the minimization with the line-search Wolfe condition [11]. The gradient descent may be trapped in local minima. To find a good local minima, we compute the gradient descent with about 10 random initializations and we keep the solution \tilde{x}_n which minimizes the error $\mathcal{E}(\tilde{x}_n)$.

Section 4.3 shows that $\hat{C}x(k, k', \lambda, \lambda')$ is a sparse matrix with non-zero coefficients when $k\lambda \approx k'\lambda'$. We compute approximations of x from a subset of these non-negligible correlation coefficients. Since $\hat{C}x$ is symmetric, we can impose $|\lambda| \geq |\lambda'|$. The wavelet frequencies λ and λ' correspond to scales $2^{j/Q} \sim |\lambda|^{-1}$ and $2^{j'/Q} \sim |\lambda'|^{-1}$. In dimension d , a signal of N^d samples has at most $\log_2 N$ dyadic scales 2^j . We limit the range Δ of scale interactions by imposing that

$$j/Q \leq j'/Q \leq j/Q + \Delta \leq \log_2 N , \quad (48)$$

with $1 \leq \Delta \leq \log_2 N$.

Section 4.3 shows that non-negligible coefficients satisfy

$$|k\lambda - k'\lambda'| \leq \beta (|k|\,|\lambda| + |k'|\,|\lambda'|) \quad (49)$$

where $k\beta|\lambda|$ and $k'\beta|\lambda'|$ is replaced respectively by $\beta|\lambda|$ or $\beta|\lambda'|$ if $k = 0$ or $k' = 0$. Since λ and λ' are in the same half space, we can restrict ourself to $k \geq 0$ and $k' \geq 0$. Given that $|\lambda| \geq |\lambda'|$, to correlate λ with λ' we choose $k = 0$ or $k = 1$ and adjust the value of k' to satisfy (49).

Let M be the total number of correlation coefficients which satisfy (49) and (48), plus the number of integral coefficients $\hat{I}x$. A complex number is counted as two coefficients. For one-dimensional signals, the value of M depends upon the range of scales Δ and the number Q wavelet scales per octave, and one can verify that:

$$M \sim \Delta^2 Q^2 \log_2 N \text{ with } \Delta \leq \log_2 N . \quad (50)$$

For images, it depends upon the number L of angles. One can verify that $M \sim \Delta^2 L^2 \log_2 N^2$. Next section studies the reconstruction of signals from these M invariants coefficients.

5.2 Numerical Reconstruction Results

Reconstructions \tilde{x} are computed up to an unknown translation, from M invariant coefficients, with the gradient descent algorith. We register these reconstruction with a global translation which minimizes the Euclidean distance with the original signal x . The reconstruction error is evaluated by the Peak Signal to Noise ratio in db

$$\text{PSNR}(x, \tilde{x}) = 20 \log_{10} \frac{N^{d/2} \max_u |x(u)|}{\|x - \tilde{x}\|_2} .$$

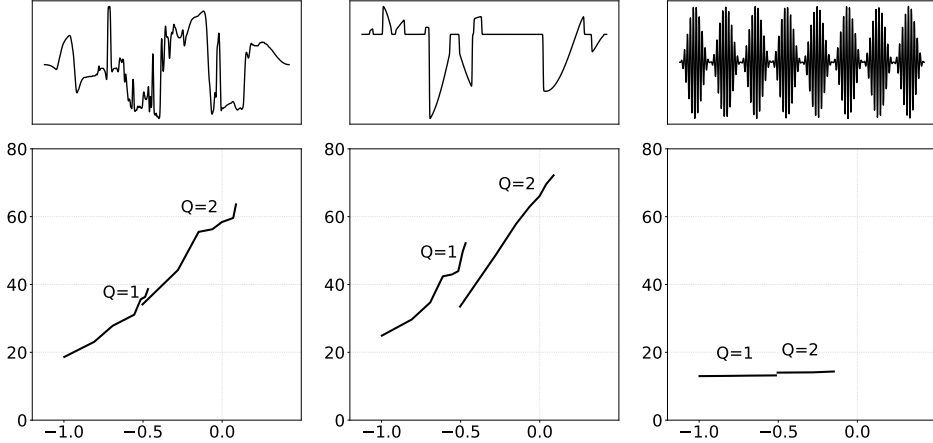


Figure 7: For each figure, the top graph is the original signals x of $N = 1024$ points. The curve below gives PSNR of signals \tilde{x} reconstructed from M wavelet harmonic correlations and integral coefficients, as a function of $\log_{10} M/N$. The first and second parts of each curve correspond to $Q = 1$ and $Q = 2$ respectively, for Δ varying.

Above 35db, reconstructed images are visually identical to the original ones and signals plots superimpose so we do not display reconstructed signals. Figure 7 gives the PSNR error as a function of the $\log_{10} M/N$ for one dimensional signals, and Figure 8 as a function of the $\log_{10} M/N^2$ for images. The number of coefficients M varies by adjusting the range Δ of scale interactions.

Figure 7 gives two examples of one-dimensional signals x having many sharp transitions, where the reconstruction \tilde{x} converges to x with a high PSNR. The approximation error has a decay

$$\|\tilde{x} - x\|_2 \leq C M^{-\chi}, \quad (51)$$

with $\chi \approx 2$. This decay exponent is surprisingly large. Indeed, the algorithm approximates x from M coefficients which are chosen independantly of x , and thus involves no adaptivity. A non-adaptive approximation in an orthonormal basis yields a much slower error deay rate. Consider the approximation of a signal x as a linear combination of M orthogonal basis vectors which are chosen independantly of x . For piecewise regular signals x having

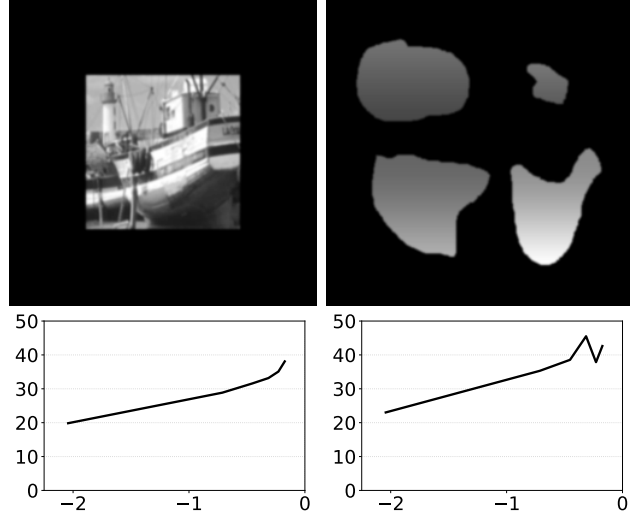


Figure 8: Each original image x shown at the top has $N^2 = 256^2$ pixels. The curve below gives the PSNR of signals \tilde{x} reconstructed from M wavelet harmonic correlations and integral coefficients, as a function of $\log_{10} M/N^2$.

discontinuities at unknown locations, when M increases the approximation error has a decay exponent $\chi \leq 1$ in all orthogonal bases [9].

On the other hand, not all signals can be represented from phase harmonic correlations. The signal at the right of Figure 7 is

$$x(t) = (1 - \cos(\epsilon t)) \cos(\lambda t) \quad \text{with } \epsilon \ll \lambda. \quad (52)$$

The cosine of frequency λ has an amplitude modulation of frequency ϵ . This amplitude modulation is not captured by the correlation of the phase harmonic coefficients of $x \star \psi_\lambda$ with $[x \star \psi_{\lambda'}]^k$ with $\lambda' = \epsilon$ because $x \star \psi_\epsilon = 0$. Indeed $\widehat{x}(\omega) = 0$ for ω in the support of $\widehat{\psi}_\epsilon$. This loss of information does not occur in the first two examples of Figure 7, because $x \star \psi_{\lambda'}(u)$ does not vanish if $x \star \psi_\lambda(u)$ is not zero at higher frequencies $\lambda > \lambda'$. This is the case when large amplitude wavelet coefficients propagate across scales and frequencies, as illustrated in Figure 2. Correlations with lower frequencies then provide the necessary information to recover $x \star \psi_\lambda$.

For images, Figure 8 shows similar results as in Figure 7. The reconstruction \tilde{x} converges to the original signal with a high PSNR, for natural images and piecewise regular cartoon images. In Figure 8 we use images of

compact support and N^2 is the total number of pixels in the image. These images have sparse representations over bump steerable wavelets. The error decay (51) has an exponent $\chi \approx 1/2$. This is the same error decay as the one obtained when approximating such discontinuous image from M vectors chosen in an orthonormal basis, independantly from the signal x . As in Figure 7, if $x * \psi_\lambda(u)$ has an amplitude modulation at a low frequency ϵ with $x * \psi_\epsilon = 0$ then such an amplitude modulation can not be reconstructed. This is typically not the case for natural images but such functions can be constructed.

These numerical examples show that one can efficiently approximate large classes of one-dimensional signals and images from a limited number M of wavelet phase harmonic integrals and correlations. However, the mathematical properties of these reconstructions remains to be understood. The oscillatory example show that not all signals can be recovered by this translation invariant representation. Moreover, the number M of non-negligible coefficients grows at most like $(\log_2 N)^3$ so when N is too large we will not have enough coefficients to reconstruct the signal. Good approximations can only be expected when M/N is not too small.

References

- [1] J. Morlet A. Grossmann, R. Kronland-Martinet. Reading and understanding continuous wavelet transforms. In *Wavelets, time-frequency representations and phase space*. Ed. J.M Combes, 1989.
- [2] E. J. Akutowicz. On the determination of the phase of a fourier integral. *Trans. of the American Mathematical Society*, 83(1):179–192, 1956.
- [3] Jan Chorowski, Ron J. Weiss, Rif A. Saurous, and Samy Bengio. On using backpropagation for speech texture generation and voice conversion. In *2018 IEEE International Conference on Acoustics, Speech and Signal Processing, ICASSP 2018, Calgary, AB, Canada, April 15-20, 2018*, pages 2256–2260, 2018.
- [4] Leon Gatys, Alexander S Ecker, and Matthias Bethge. Texture synthesis using convolutional neural networks. In C. Cortes, N. D. Lawrence, D. D. Lee, M. Sugiyama, and R. Garnett, editors, *Advances in Neural*

Information Processing Systems 28, pages 262–270. Curran Associates, Inc., 2015.

- [5] S. Jaffard. Pointwise smoothness, two-microlocalisation and wavelet coefficients. *Publications Matematiques*, 35:155–168, 1991.
- [6] Arta A. Jamshidi and Michael J. Kirby. Examples of compactly supported functions for radial basis approximations. In *International Conference on Machine Learning*, 2006.
- [7] Yann LeCun, Yoshua Bengio, and Geoffrey E. Hinton. Deep learning. *Nature*, 521(7553):436–444, 2015.
- [8] Stéphane Mallat. Zero-crossings of a wavelet transform. *IEEE Trans. Information Theory*, 37(4):1019–1033, 1991.
- [9] Stéphane Mallat. *A Wavelet Tour of Signal Processing: The Sparse Way, 3rd Edition*. Academic Press, 2001.
- [10] Stéphane Mallat. Understanding deep convolutional networks. *CoRR*, abs/1601.04920, 2016.
- [11] Jorge Nocedal and Stephen J. Wright. *Numerical Optimization*. Springer, New York, NY, USA, second edition, 2006.
- [12] Javier Portilla and Eero P. Simoncelli. A parametric texture model based on joint statistics of complex wavelet coefficients. *International Journal of Computer Vision*, 40:49–71, 2000.
- [13] Eero P Simoncelli and William T Freeman. The steerable pyramid: A flexible architecture for multi-scale derivative computation. In *IEEE INT'L CONF ON IMAGE PROCESSING*, pages 444–447. IEEE Signal Processing Society, 1995.
- [14] M. Unser, N. Chenouard, and D. Van De Ville. Steerable pyramids and tight wavelet frames in $l_2(\mathbb{N}^d)$. *IEEE Transactions on Image Processing*, 20(10):2705–2721, October 2011.
- [15] I. Ustyuzhaninov*, W. Brendel*, L. Gatys, and M. Bethge. What does it take to generate natural textures? Apr 2017.